Al- and OH-related paramagnetic impurity centres in UV- or x-irradiated $ZnWO_4$ single crystals

2003 J. Phys.: Condens. Matter 15 7073

(http://iopscience.iop.org/0953-8984/15/41/015)

INSTITUTE OF PHYSICS PUBLISHING JOURNAL OF PHYSICS: CONDENSED MATTER

J. Phys.: Condens. Matter **15** (2003) 7073–7084 PII: S0953-8984(03)65276-8

Al- and OH-related paramagnetic impurity centres in UV- or x-irradiated $ZnWO_4$ single crystals

A Watterich[1], A Hofstaetter[2], A Scharmann[2] and O Szakács[1]

[1] Research Institute for Solid State Physics and Optics, Hungarian Academy of Sciences, Konkoly-Thege M. út 29-33, Budapest, H-1121, Hungary
[2] 1.Physics Institute, Justus-Liebig-University, Heinrich-Buff-Ring 16, Giessen, D-35392, Germany

Received 24 June 2003
Published 3 October 2003
Online at stacks.iop.org/JPhysCM/15/7073

Abstract

Using electron paramagnetic resonance (EPR) and in one case also electron nuclear double resonance new trapped electron and hole centres are characterised in $ZnWO_4$ single crystals. In undoped and Al-doped $ZnWO_4$ a new W^{5+}-type defect is produced by UV- or x-irradiation at 77 K. The centre is stabilised by a nearby Al^{3+} impurity that is substituting for Zn^{2+}. In $ZnWO_4$:Al in addition to the above electron-type defect three kinds of hole-type centres created by x-irradiation at 77 K are also studied: one of these is assigned to an O^- ion near a V_{Zn}–Al^{3+}_{Zn} complex, and the second to an O^- ion near a V_{Zn}–OH^- pair. The $\tilde{\mathbf{g}}$- and hydrogen super hyperfine (SHF) tensors of the latter centre have been published previously. Due to the higher concentration in the Al-doped crystal, SHF tensors of two W neighbours could also be determined. The third hole-type defect shows quartet SHF ($I = 3/2$) with a 100% abundant nucleus and therefore the O^- in this centre is most likely stabilised by an Na^+ impurity. Complete sets of EPR parameters are compared for trapped electron and trapped hole centres including previously characterised defects.

1. Introduction

$ZnWO_4$ is known not only as a radiation detector [1–3]; it is also a good model material with low symmetry. The study of radiation-induced defects is important in understanding radiation damage effects and in addition the knowledge and comparison of the structure of the large number of observable paramagnetic defects allow a deeper insight into the defect structure. Since in $ZnWO_4$ the magnetic isotopes of the host nuclei contributing to super hyperfine (SHF) interactions have low abundance, the electron paramagnetic resonance (EPR) lines are usually fairly narrow and therefore easily detectable even for small centre concentrations. Because of the narrow lines the EPR spectra are usually well resolved and the spin-Hamiltonian parameters can be determined fairly accurately. Using these data and comparing other features reliably, models can be given serving as good bases for future theoretical calculations.

The raw materials of $ZnWO_4$ usually contain traces of a large number of impurities (Pb, Cr, Mg, Fe, Si, Al, Ca, Cu and Sn [4]). In our samples previously we have shown the presence of Cr^{3+}, Mn^{2+}, Fe^{3+}, Fe^{2+}, Co^{2+}, Cu^{2+}, Mo^{6+}, Rh^{2+}, Pt^{3+}, Sn^{4+} and two kinds of OH^- ions: substitutional OH^- replacing O^{2-} and OH^- accompanied with a zinc vacancy (V_{Zn}) [5, 6]. The substitutional OH^- ions compensate monovalent cation impurities [7], while the concentration of OH^-–V_{Zn} dipoles is enhanced by doping with trivalent cations (for example Fe^{3+} and Al^{3+} [6]). The cation impurities mentioned above substitute for Zn^{2+} ions except Mo^{6+}, which replaces W^{6+}. Quite a few of these impurities are known as trapping centres.

One group of radiation damage defects is of electron-type. In undoped $ZnWO_4$ single crystals electrons are trapped at oxygen vacancies which may be in two positions (named A or B). These intrinsic defects have been created by energetic electron irradiation at ∼300 K, and are denoted as $V_O^{\bullet}$(A) and $V_O^{\bullet}$(B) centres [8], respectively. In the presence of appropriate compensators the electron may be localised on one W or Mo forming essentially a W^{5+} or Mo^{5+} centre. The identified charge compensating impurities were Sn^{4+} replacing Zn^{2+} ions (W^{5+}–Sn_{Zn}^{4+} [4]) and OH^- replacing O^{2-} ions (W^{5+}–H and Mo^{5+}–H [7]). The second type of observed defects is of hole-type: the self-trapped hole is essentially an O^- ion without any local charge compensation and is stable below 70 K [9]. In other hole-type defects the O^- ions were stabilised either by monovalent impurity ions (Li [10]) or nearby V_{Zn} [8], impurity–V_{Zn} complexes (like V_{Zn}–OH^- [11] or V_{Zn}–Tm^{3+} pairs [12]).

In this work we report a new W^{5+}-type defect where a nearby Al^{3+} impurity stabilises the centre produced by UV- or x-irradiation at 77 K in undoped and Al-doped $ZnWO_4$ single crystals. Comparison of its spin-Hamiltonian parameters with those of the previously known W^{5+}–Sn_{Zn}^{4+} centre lead to a modified model of the latter defect. In the doped crystal, in addition to the above electron-type defect, three different hole-type centres that are created by x-irradiation at 77 K are studied and compared. All defects are characterised by EPR while electron nuclear double resonance (ENDOR) spectroscopy was used to identify the Al impurity as part of the electron-type centre.

2. Experimental methods and crystal structure

Single crystals of $ZnWO_4$ were grown in Pt crucibles in air using a balance-controlled Czochralski technique [13]. The raw materials were analytical grade ZnO (REANAL) and WO_3 chemically produced from analytical grade Na_2WO_4 [14]. EPR and ENDOR measurements were carried out using a BRUKER Spectrometer (Model ESP 300 E) in Giessen (Germany). An x-ray source was employed using 150 kV and 20 mA with irradiation times up to 1 h. For UV illuminations at 365 nm, a low-power Hg lamp with appropriate filter was employed. To fit the experimental data the computer program 'VisualEPR' developed by V Grachev was used.

Zinc tungstate is a monoclinic crystal with space group $C_{2h}^4(P2/c)$ [15, 16]. The two zinc and two tungsten ions in a unit cell are magnetically equivalent, having C_2 local symmetry. Impurity centres at Zn or W sites without any nearby lattice defects preserve the original C_2 symmetry of the lattice site and give only one EPR spectrum for an arbitrary orientation of the magnetic field **B**. If the centre is accompanied by a nearby imperfection of the lattice, the local symmetry will be reduced to C_1 and therefore the number of spectra is increased to two in accordance with the two geometrically different defect sites. However, for **B** oriented in the (010) plane or along crystallographic axes the two spectra are superposed. There are two different oxygen sites: one has in its closest neighbourhood two Zn and one W (named A) cations, and the other has two W and one Zn (named B) cations; both sites have C_1 local symmetry.

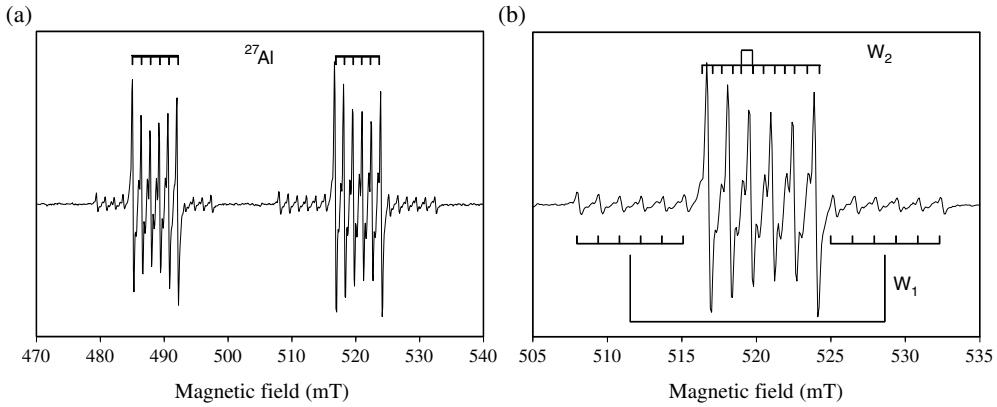

Figure 1. EPR spectrum of the W^{5+}–Al^{3+}_{Zn} centre measured at ∼13 K and 9.5 GHz in a $ZnWO_4$ single crystal after 366 nm irradiation at 77 K for a general direction of **B**: polar angles with respect to the [100] and [001] axes are $\phi = 39.63°$ and $\theta = 45°$, respectively. Stick diagrams indicate (a) the ^{27}Al and (b) the two different ^{183}W SHF satellites.

3. Results and discussion

3.1. EPR of the electron-type defect

After UV- or x-irradiation at 77 K in $ZnWO_4$ single crystals a new electron-type defect is observed in addition to the previously published W^{5+} centre coupled to an Sn impurity (W^{5+}–Sn^{4+}_{Zn}) [5]. For an arbitrary orientation of the magnetic field **B** in the (100) and (001) planes, resonances of the new centre split into two branches which coincide if **B** is parallel to any crystal axis or is in the (010) plane. Thus the centre has C_1 symmetry. The spectra show sextet SHF splittings (figure 1(a)) by a nucleus with $I = 5/2$ and 100% relative abundance. There are only four elements with these characteristics: ^{27}Al, ^{55}Mn, ^{127}I and ^{141}Pr. It is unlikely that the latter two elements were impurities in $ZnWO_4$; however, Mn^{2+} is observable by EPR and Al could also be identified by atomic absorption spectroscopy and cathodo-luminescence [17] as an impurity in many samples. Since Al doping substantially enhanced the intensity of the EPR spectra, this SHF interaction was assigned to the ^{27}Al nucleus. Our ENDOR studies described below proved this assignment.

The ^{27}Al SHF interaction will split all EPR lines including SHF satellites due to other nuclei into six. Around each of the large sextet lines, two sets of weaker doublets (their intensities are about 12 times smaller than the main lines) are observable. These resonances are due to interactions with ^{183}W nuclei ($I = 1/2$ and abundance 14.3%). The nuclei involved in stronger and weaker interactions are named W_1 and W_2, respectively (figure 1(b)).

For the determination of the spin-Hamiltonian parameters of the Al-related electron centre, angular variations of the EPR spectra were observed by rotating the magnetic field in three different planes. The spin Hamiltonian employed was

$$H_s = \mu_B \mathbf{S} \cdot \tilde{\mathbf{g}} \cdot \mathbf{B} + \sum (\mathbf{S} \cdot \tilde{\mathbf{A}}_i \cdot \mathbf{I}_i - g_{Ni}\mu_{Ni}\mathbf{B} \cdot \mathbf{I}_i) \quad (1)$$

where i denotes a specific interacting nucleus of W_1 or Al, $S = 1/2$, $I_i = 1/2$ or 5/2, respectively, and $\tilde{\mathbf{A}}_i$ represents the corresponding SHF interaction tensor. The optimised spin-Hamiltonian parameters of the new centre are shown in table 1. Angular variations of the ^{27}Al and the $^{183}W_1$ SHF EPR lines for one plane are shown in figures 2(a) and (b), respectively. Because of poor resolution the angular variations of the $^{183}W_2$ SHF lines could not be fitted.

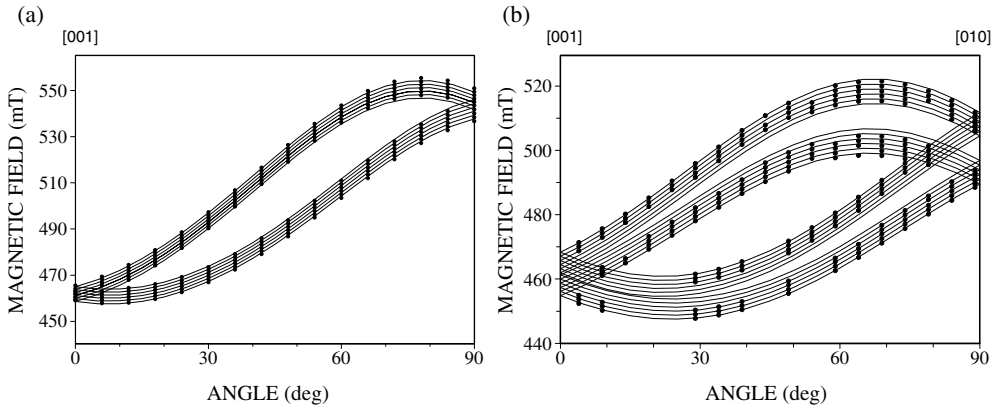

Figure 2. EPR angular variations for the W^{5+}–Al^{3+}_{Zn} centre in a $ZnWO_4$ single crystal (the lines of both geometrical sites are presented): (a) angular variation of ^{27}Al SHF lines around [110], (b) that of W_1 SHF lines rotating **B** around the [100] direction. Symbols represent experimental data and the solid curves are computer-simulated angular variations calculated with the optimized spin-Hamiltonian parameters. Observations were made at ∼13 K and 9.5 GHz.

(Therefore the index of W_1 will be omitted if W itself is an index.) In figures 2(a) and (b) symbols represent experimental data and the solid curves are computer-simulated angular variations calculated using the computer-fit spin-Hamiltonian parameters.

Since the features of the Al-related centre are very similar to those of W^{5+}–Sn^{4+}_{Zn}, we will follow the discussion given in [5]. The principal g-values of the new centre are smaller than the free electron value ($g_e = 2.0023$), typical for an electron-type defect. Because of $S = 1/2$, the large g shift and the strong spin density on one W nucleus the new centre is essentially a W^{5+} centre, whose electron configuration is $5d^1$. Indeed, the principal values and eigenvectors of the $\tilde{\mathbf{g}}$ and the $\tilde{\mathbf{A}}$ W HF tensor of the new centre are much closer to those of the W^{5+}–H and W^{5+}–Sn^{4+}_{Zn} centres than to those of the vacancy-related $V^{\bullet}_{O}$(B) centre (table 1). The latter was modelled as an electron trapped at an anion vacancy between two W sites with its spin density more equally distributed on two neighbouring W nuclei.

It is useful to transform the values of HF and SHF interactions with W and Al nuclei into the following form: $\tilde{\mathbf{A}} = A_{iso}\tilde{\mathbf{1}} + \tilde{\mathbf{B}}$, where A_{iso}, $\tilde{\mathbf{1}}$ and $\tilde{\mathbf{B}}$ are the isotropic hyperfine coupling constant (given by $A_{iso} = -8\pi/3|\Psi(0)|^2\mu_B\mu_N$, where $|\Psi(0)|^2$ is the spin density at the nucleus), the unit tensor and the traceless tensor of the anisotropic hyperfine coupling, respectively. The diagonalized components are $B_{xx} = -b + b'$, $B_{yy} = -b - b'$ and $B_{zz} = 2b$, where b is the axial part and b' is the measure of the deviation from axial symmetry. The experimental hyperfine data (which in addition have to be corrected for the different nuclear magnetic moments of ^{183}W and ^{27}Al) show that the spin density at the W_1 nucleus is greater than at the Al nucleus, similar to the situation in the W^{5+}–Sn^{4+}_{Zn} centre. Therefore the defect is described as a W^{5+} with a perturbation by Al^{3+} substituting for Zn^{2+} (rather than W^{6+}) and is classified as W^{5+}–Al^{3+}_{Zn}. The dominant isotropic part in the Al SHF interaction shows that the wavefunction of the defect electron overlaps with the Al^{3+} neighbour, giving rise to a contact interaction either due to direct density at the Al nucleus or due to spin polarisation. In the unirradiated crystal the Al^{3+} impurity needs charge compensation. This can be realised either non-locally by a V_{Zn}–OH^- complex (the presence of such complexes was proven by IR spectroscopy [6]), or locally or non-locally by a zinc vacancy. In the new radiation-induced electron-type centre it is very likely that an isolated Al^{3+}_{Zn} (without local charge compensation)

Table 1. Optimised spin-Hamiltonian parameters of the W^{5+}–Al^{3+}_{Zn} centre are presented for comparison with the principal g-values and eigenvectors of the $V^{\bullet}_{O}$ (B), W^{5+}–H and Mo^{5+}–H centres in $ZnWO_4$ single crystals. Direction cosines of the dimensionless eigenvectors are defined with respect to the crystallographic axes [100], [010] and [001], respectively. Estimated uncertainties for eigenvector components of the $\tilde{\mathbf{g}}$, $\tilde{\mathbf{A}}_{W1}$ and $\tilde{\mathbf{A}}_{Al}$ tensors for the W^{5+}–Al^{3+}_{Zn} centre are ±0.003, ±0.003 and ±0.003, respectively.

	$\tilde{\mathbf{g}}$			$\tilde{\mathbf{A}}_{W\text{ or }Mo}$ (HF) ($\times 10^{-4}$ cm^{-1})			$\tilde{\mathbf{A}}_{Al\text{ or }Sn\text{ or }W}$ (SHF) ($\times 10^{-4}$ cm^{-1})			
Centre	g_{xx}	g_{yy}	g_{zz}	A_{xx}	A_{yy}	A_{zz}	A_{xx}	A_{yy}	A_{zz}	References
	1.3281±	**1.4926±**	**1.1674±**	**91.3 ± 2**	**46.1 ± 2**	**150.6 ± 2**	**8.6 ± 1**	**8.8 ± 1**	**10.0 ± 1**	
	0.0004	**0.0004**	**0.0004**							
W^{5+}–Al^{3+}_{Zn}	−0.060	−0.034	0.998	0.278	−0.043	0.959	0.775	−0.337	0.534	This work
	−0.060	−0.389	0.042	0.945	0.193	−0.266	−0.373	0.438	0.818	
	0.386	0.921	0.054	−0.174	0.980	0.094	0.510	0.833	−0.213	
	1.4675	**1.6323**	**1.3821**	**73.1**	**52.3**	**126**	**443.6**	**448.5**	**463.7**	
W^{5+}–Sn^{4+}_{Zn}	−0.014	−0.162	0.987	0.478	−0.283	0.831	−0.120	−0.383	0.916	[5]
	0.753	−0.651	−0.096	0.738	−0.383	−0.555	0.987	−0.144	0.069	
	0.658	0.742	0.131	0.476	0.879	0.026	0.106	0.912	0.396	
	1.4911	**1.3718**	**1.1513**	**58.5**	**61.3**	**148.7**				
W^{5+}–H	0.163	−0.282	0.946	0.52	−0.18	0.84				[7]
	0.767	−0.567	−0.301	0.81	−0.20	−0.54				
	0.621	0.774	0.124	0.26	0.96	0.04				
	1.9021	**1.8250**	**1.7021**	**28.2**	**32.0**	**79.8**	**22.2**	**26.0**	**30.0**	
Mo^{5+}–H	0.096	−0.178	0.979	0.575	−0.226	0.786	0.516	−0.850	0.116	[7]
	0.778	−0.601	−0.185	0.757	−0.217	−0.616	0.750	0.386	−0.536	
	0.621	0.779	0.081	0.310	0.950	0.046	0.413	0.359	0.837	
	1.5409	**1.571**	**1.8185**	**36.9**	**68.2**	**96.4**	**21.6**	**23.0**	**28.0**	
$V^{\bullet}_{O}$(B)	0.236	−0.105	0.966	−0.333	0.367	−0.869	0.675	−0.736	0.043	[8]
	0.825	−0.504	−0.257	0.612	−0.617	−0.495	0.707	0.629	−0.323	
	0.513	0.858	−0.032	0.717	0.697	0.019	0.211	0.249	0.945	

is involved which stabilises the extra charge of W^{5+}. The similarity of the g principal and eigenvector values of the Al-perturbed electron centre to those of related centres supports this model (table 1).

It should be pointed out that the spin density at the central W nucleus is larger than in the other related centres, even than in the W^{5+}–Sn^{4+}_{Zn} centre. From simple point charge considerations the attraction of the electron away from the W site should be stronger for an Sn^{4+} neighbour than for an Al^{3+}, if everything else were the same. The hyperfine interaction reveals the opposite. This result can be understood by the assumption that the Sn^{4+} substituting for Zn^{2+} is charge compensated by a Zn vacancy. Such an Sn^{4+}–V_{Zn} complex would be electrically neutral with respect to the perfect lattice. The impurity that is part of the polarised Sn^{4+}–V_{Zn} dipole, however, would still attract the electron mainly localised at W, but less than a single Al^{3+} ion whose additional compensating positive charge is non-local. The modified model for the Sn related defect is therefore a W^{5+}–Sn^{4+}_{Zn}–V_{Zn} centre.

Two final remarks on this W^{5+}–Al^{3+}_{Zn} centre:

(a) Just like in the W^{5+}–Sn^{4+}_{Zn} centre a weaker SHF interaction (W_2) from a more distant W ion is observed, too.

(b) The production of the defect by UV illumination at 77 K can be explained in the same way

as in [7]: 366 nm illumination will excite Fe^{2+} ions (broad optical absorption peaking at 460 nm) and liberate electrons which are then captured at W^{6+} ions near Al^{3+} impurities. This mechanism is suggested by the enhanced concentration of Fe^{3+} ions observed by EPR after UV illumination.

3.2. ENDOR of the electron-type defect

In order to prove the nature of the perturbing impurity in the W^{5+}–Al^{3+}_{Zn} defect in $ZnWO_4$ we performed additional ENDOR measurements. Figure 3 shows the ENDOR spectra obtained on the six SHF EPR lines ($m_I = 5/2, 3/2, 1/2, -1/2, -3/2, -5/2$, corresponding magnetic field values indicated).

ENDOR frequencies of a system with $S = 1/2$ and $I \geqslant 14$ in axial symmetry are given by

$$\nu = |m_S[A_{\rm iso} + b(3\cos^2\theta - 1)] - \nu_{\rm N} + m_q Q(3\cos^2\Phi - 1)| \qquad (2)$$

where $m_S = \pm 1/2$, $\nu_{\rm N}$ is the nuclear Larmor frequency, Q the nuclear quadrupole splitting constant, and θ and ϕ are the angles between the magnetic field and the relevant tensor axes, respectively [18]. $m_q = 1/2(m'_I + m_I)$ is given by the average of the quantum numbers involved in the nuclear transitions. For a given orientation with actual hyperfine and quadrupole values A and Q' the two possible m_S values give rise to two groups of ENDOR lines, centred at $|A|/2$, separated by $\Delta\nu = 2 \cdot \nu_{\rm N}(B)$ and further shifted by $2 \cdot m_q \cdot |Q'|$. This explains the characteristic structure of the ENDOR spectra: from the $m_I = 5/2$ and $-5/2$ only one neighbouring nuclear level can be reached by a $\Delta m_I = \pm 1$ transition, so only one ENDOR line at a frequency corresponding to $m_q = 2$ respectively $m_q = -2$ is observed, whereas from the other nuclear states ($m_I = \pm 3/2, \pm 1/2$) two transitions are always allowed (with $m_q = \pm 2, \pm 1$ for $m_I = \pm 3/2$ and $m_q = \pm 1, 0$ for $m_I = \pm 1/2$).

To determine the interacting nucleus from the ENDOR spectra we had to take the experimentally observed separations $\Delta\nu$, divide by 2 and normalise to a constant field of 350 mT (figure 4). They are then clearly centred around $\nu_{\rm N,Al}$ ($B = 350$ mT) $= 3.89$ MHz, whereas the other candidates with $I = 5/2$ and 100% abundance would give a noticeably different result (for $B = 350$ mT, $\nu_{\rm N,Mn} = 3.69$ MHz, $\nu_{\rm N,}I = 3.00$ MHz and $\nu_{\rm N,Pr} = 4.00$ MHz).

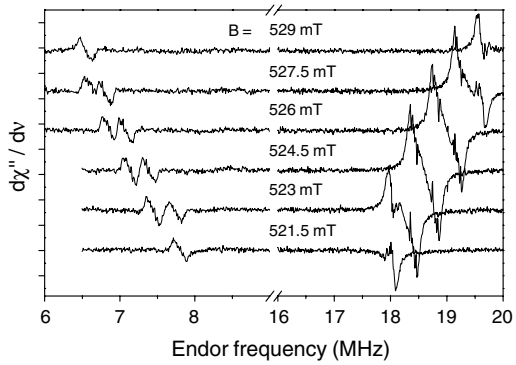

Figure 3. ENDOR lines of the W^{5+}–Al^{3+}_{Zn} centre in a $ZnWO_4$ single crystal (for an arbitrary orientation of the magnetic field). The measurement was made at 8 K. Each of the six SHF EPR lines ($m_I = 5/2, 3/2, 1/2, -1/2, -3/2, -5/2$) was in turn saturated (the magnetic field values are indicated).

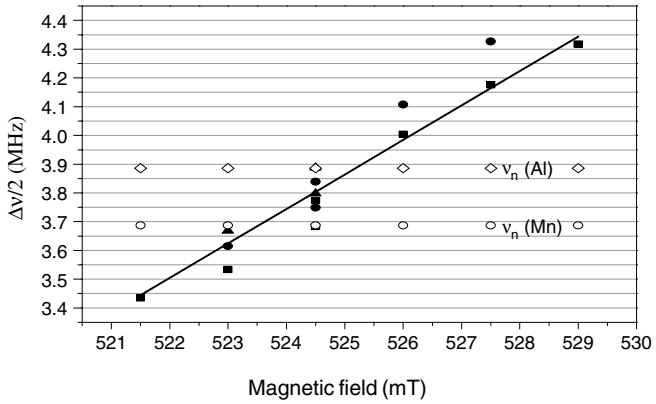

Figure 4. Half-differences of ENDOR frequencies ($\Delta\nu/2$) of each ENDOR line between $m_S = 1/2$ and $-1/2$, presented (full symbols, normalized for 350 mT) as the function of the magnetic fields where saturation was made. The Larmor frequencies of ^{27}Al and ^{55}Mn nuclei are also shown at each magnetic field (open symbols).

3.3. EPR of hole-type defects

In the $ZnWO_4$:Al sample under investigation, in addition to the two electron centres described above several other paramagnetic centres are observed after x-irradiation at 77 K. Among them are two very intense hole-type defects and a third type with a quartet SHF. All three centres have C_1 symmetry.

One of the intense spectra has already been identified as being due to an O^- trapped at a V_{Zn}–OH^- complex, denoted as O^-–V_{Zn}–OH^- [11]. However, in the $ZnWO_4$:Al system its intensity was extremely high, since the V_{Zn}–OH^- complex charge compensating the Al^{3+} impurity non-locally is available in a relatively high concentration [6]. This allowed the additional determination of the SHF interaction tensors for two regular W neighbours. The second intense spectrum can be produced only in Al-doped samples and partly overlaps that of the O^-–V_{Zn}–OH^- centre. The shapes and angular dependences of these spectra (figure 5(a) and (b)) are very similar to those of the O^-–V_{Zn}–OH^- centre; however, the effective g-values are slightly shifted and therefore many of the EPR lines are clearly distinguishable. We will denote the new hole-type defect hereafter as an O^-–V_{Zn}–Al^{3+} centre. We assume the participation of a zinc vacancy in this complex since both an isolated Al^{3+} and O^- locally represent net positive charges compared with the perfect lattice and such vacancies typically provide charge compensation for heterovalent impurities in $ZnWO_4$. In the EPR spectrum of both centres three ^{183}W SHF splittings show up (two of them well resolved), identified again on the basis of intensity ratios of the main and SHF lines which reflect the natural abundance of the corresponding nucleus (^{183}W). In figure 5(a) the main lines of both centres (all lines of the O^-–V_{Zn}–OH^- centre are doubled because of the proton SHF interaction) and the hyperfine lines arising from three different W neighbours are marked (as A_1, A_2, A_3 for O^-–V_{Zn}–OH^- and A'_1, A'_2, A'_3 for O^-–V_{Zn}–Al^{3+} centres). Figure 5(b) shows the same spectrum but magnified. Here are shown also those satellites (marked $A_1 + A_2$, $A_1 + A_3$, $A_2 + A_3$ and $A'_1 + A'_2$, $A'_1 + A'_3$, $A'_2 + A'_3$, respectively) that arise from centres where *two* of the tungsten neighbours have ^{183}W nuclei. The relative intensity ratio of these lines compared to the main lines is 0.69% as expected form the natural abundance of ^{183}W, but more important is the fact that they are unambiguously identified as due to W by the size of the splitting (e.g. $A_1 + A_2$) since possible ^{67}Zn ($I = 5/2$, abundance 4.1%) SHF lines would be expected with close intensity ratios

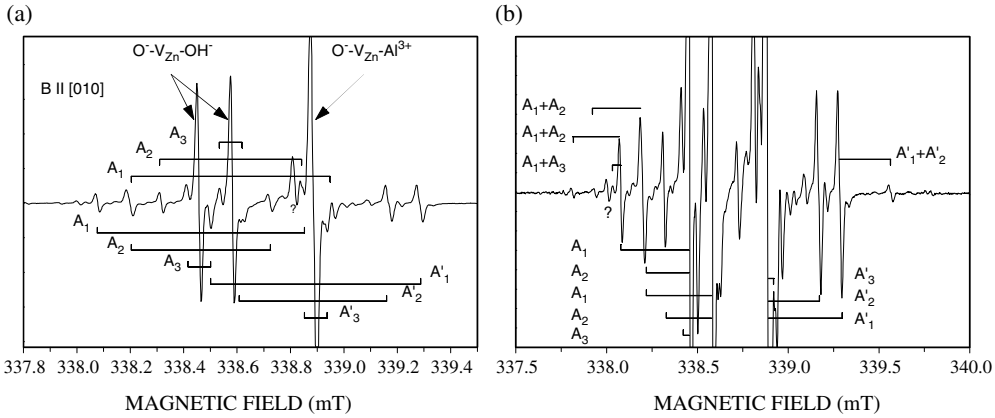

Figure 5. EPR spectra of the O^-–V_{Zn}–OH^- and O^-–V_{Zn}–Al^{3+} centres in $ZnWO_4$:Al single crystal after x-irradiation at 77 K, measured at 30 K and 9.5 GHz. (a) The main lines of the centres are marked and stick diagrams indicate the splittings due to three different ^{183}W SHF interactions (marked A_1, A_2, A_3 and A'_1, A'_2, A'_3 for O^-–V_{Zn}–OH^- and O^-–V_{Zn}–Al^{3+} centres, respectively). (b) The same spectrum but magnified. The stick diagrams of the outermost EPR lines arise from *one* W nucleus (marked A_1, A_2, A_3 and A'_1, A'_2, A'_3 for O^-–V_{Zn}–OH^- and O^-–V_{Zn}–Al^{3+} centres, respectively) or simultaneous SHF interactions with *two* ^{183}W nuclear spins (marked $A_1 + A_2$, $A_1 + A_3$, $A_2 + A_3$ and $A'_1 + A'_2$, $A'_1 + A'_3$, $A'_2 + A'_3$, respectively).

(0.71%). All other lines that appear in figure 5(b) in the low and high field parts where the two spectra do not overlap have relative intensities much smaller or much larger than 0.71%. These lines do not belong to the corresponding centres (as can also be seen from their different angular dependence). So in contrast to the case of the self-trapped hole in $ZnWO_4$ [9] no Zn SHF is observed. The missing Zn SHF supports the assumption that in each of the present centres a Zn vacancy is nearby. For both hole centres angular dependencies of the spectra were measured in three different planes and fitted to the spin-Hamiltonian (1) using $S = 1/2$ and $I_i = 1/2$. The optimised parameters obtained are shown in tables 2 and 3. As can be seen from figures 6(a) to (c) and 7(a) and (b) they fit the experimental results for the main, W_1 and W_2 SHF lines of the O^-–V_{Zn}–Al^{3+} centre and for the W_1 and W_2 SHF lines of the O^-–V_{Zn}–OH^- centre very well. Table 2 shows principal and eigenvector values of the ^{183}W SHF interaction tensors for both hole-type centres studied in this work, in comparison with the corresponding parameters of the self-trapped hole. While the SHF principal values of both perturbed centres agree within experimental error, the corresponding values for the self-trapped holes are slightly smaller. This deviation can be explained on the basis of the models. In the self-trapped hole centre there is a perfect lattice environment; however, in the perturbed defects a Zn vacancy is near to the O^- ion. Since the Zn vacancy has a net negative charge relative to the perfect lattice it will polarise the O^- ion: towards the Zn vacancy it will be more positive, towards the W nuclei more negative. This is why the W SHF interactions will be stronger than in the unperturbed self-trapped defect. However, the vacancy's perturbing effect will be modified (presumably slightly reduced) by the additional impurities (OH^- or Al^{3+}) which are obviously relatively far from the O^- since the proton SHF is very weak and no resolved Al SHF is measured with EPR.

The third spectrum with low intensity and quartet SHF is very probably due to an O^- ion perturbed by Na^+ ($I = 3/2$ and 100% natural abundance for ^{23}Na), since our crystals were prepared from Na_2WO_4 and very likely contain Na impurities, at least in traces. The

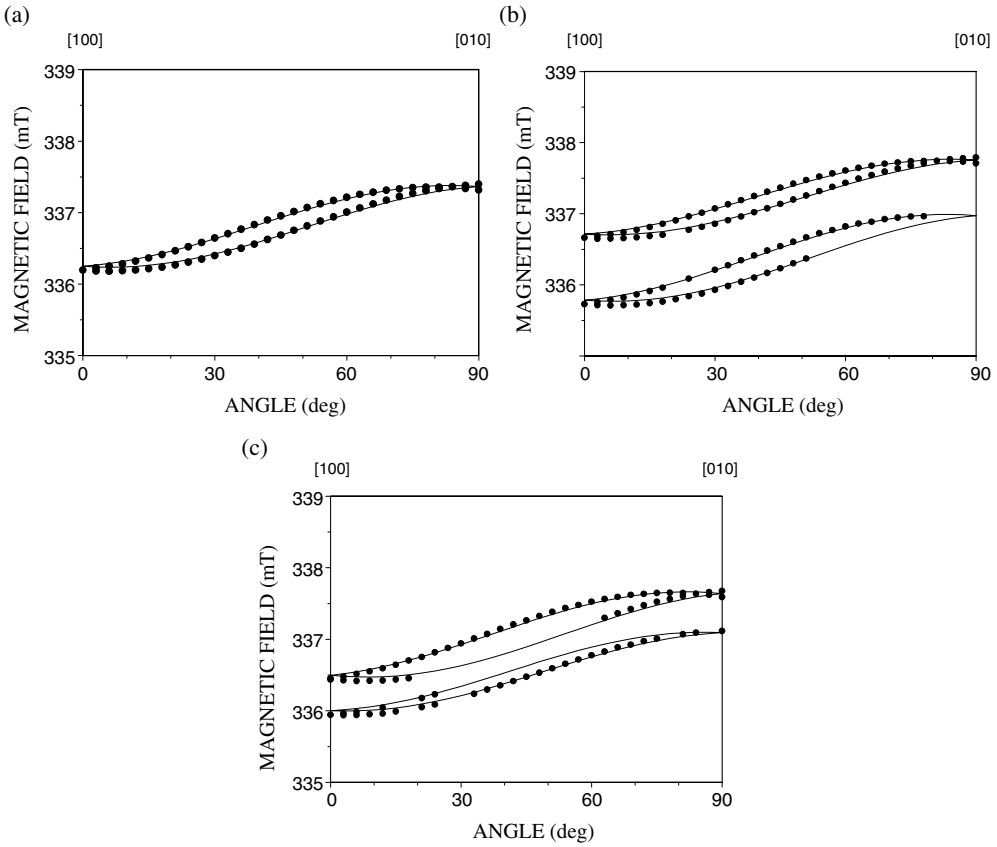

Figure 6. Angular variations of the (a) main, (b) W_1 and (c) W_2 SHF lines of the O^-–V_{Zn}–Al^{3+} centre in $ZnWO_4$:Al single crystal. Symbols represent experimental data and solid curves are computer-simulated angular variations based on optimised spin-Hamiltonians.

Table 2. SHF spin-Hamiltonian parameters of hole-type defects in $ZnWO_4$.

	$\tilde{\mathbf{A}}_1$			$\tilde{\mathbf{A}}_2$					
Centre	A_{xx}	A_{yy}	A_{zz}	A_{xx}	A_{yy}	A_{zz}	a_1	a_2	References
	4.67	**5.78**	**8.37**	**2.97**	**3.59**	**5.22**	**6.27**	**3.93**	
O^- (intrinsic)	0.468	0.699	−0.541	−0.568	0.679	0.466			[9]
	0.802	−0.593	−0.073	0.017	−0.557	0.831			
	0.372	0.399	0.838	0.823	0.479	0.304			
	6.9 ± 0.1	**8.2 ± 0.1**	**11.1 ± 0.1**	**3.0 ± 0.1**	**4.0 ± 0.1**	**6.0 ± 0.1**	**8.7**	**4.3**	
O^-–V_{Zn}–OH^-	0.462	0.703	−0.541	−0.353	0.760	0.545			This work
	0.815	−0.577	−0.055	−0.160	−0.623	0.766			
	0.351	0.415	0.839	0.922	0.183	0.341			
	6.8 ± 0.1	**8.1 ± 0.1**	**11.2 ± 0.1**	**3.4 ± 0.1**	**3.9 ± 0.1**	**6.0 ± 0.1**	**8.7**	**4.3**	
O^-–V_{Zn}–Al^{3+}	0.518	0.685	−0.513	−0.409	0.702	0.583			This work
	0.777	−0.627	−0.052	−0.126	−0.676	0.726			
	0.358	0.372	0.857	0.904	0.224	0.365			

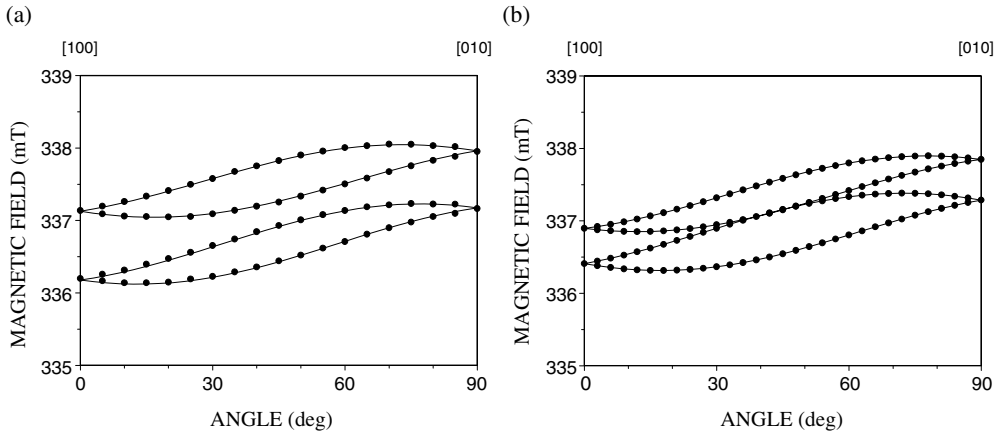

Figure 7. Angular variations of the (a) W_1 and (b) W_2 SHF lines of the O^-–V_{Zn}–OH^- centre in $ZnWO_4$:Al single crystal. Symbols represent experimental data and solid curves are computer-simulated angular variations based on optimised spin-Hamiltonians.

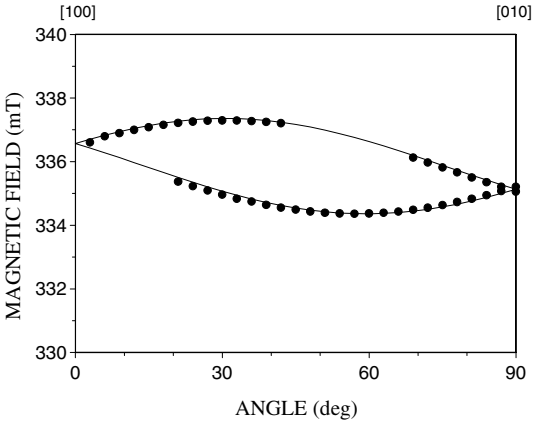

Figure 8. Angular variation of the O^-–Na^+_{Zn} defect (actually the centre of the quartet line spectrum) in one of the three measured planes.

defect is therefore denoted as O^-–Na_{Zn}. Figure 8 shows the angular dependence of resonance positions for this defect (actually the centre of the quartet line spectrum) in one of the three planes measured, and the corresponding fit with the optimised tensor parameters are presented in table 3.

The close relationship between the hole-type centres listed is demonstrated by similar spin-Hamiltonian parameters (tables 2 and 3). They all can be described primarily as O^- ions in position B, evidence for this location being given by the observation of two stronger W and one Zn SHF interactions. In its intrinsic form (self-trapped-hole) this defect is unstable above 70 K; the hole becomes mobile and will be recaptured at sites where monovalent impurities or V_{Zn}–impurity complexes stabilise the O^-, creating related centres [9]. We were now able to analyse in detail two new hole-type defects that fit into this series.

Table 3. Principal values and eigenvectors of the $\tilde{\mathbf{g}}$ tensors of various hole-type defects in $ZnWO_4$ single crystals.

Centre	g_{xx}	g_{yy}	g_{zz}	References
	2.0397	**2.0208**	**2.0030**	
O^- (intrinsic)	0.586	0.201	0.785	[9]
	0.244	0.880	−0.408	
	0.773	−0.430	−0.466	
	2.0407	**2.0195**	**2.0029**	
O^-–Li_{Zn}	0.517	0.430	0.740	[10]
	−0.057	0.880	−0.472	
	0.854	−0.202	−0.480	
	2.0435 ± 0.0002	**2.0214 ± 0.0002**	**2.0035 ± 0.0002**	
O^-–Na_{Zn}	0.503	0.079	0.861	This work
	0.329	0.903	−0.275	
	0.799	−0.421	−0.429	
	2.0448	**2.0042**	**2.0001**	
O^-–V_{Zn}	0.415	0.638	0.649	[8]
	−0.458	0.768	−0.457	
	0.786	0.107	−0.609	
	2.0495	**2.0136**	**2.0014**	
O^-–V_{Zn}–OH^-	0.464	0.588	0.663	[11]
	−0.182	0.795	−0.578	
	0.867	−0.148	−0.476	
	2.0533	**2.0107**	**2.0024**	
O^-–V_{Zn}–Tm^{3+}	0.453	0.617	0.643	[12]
	−0.176	0.769	−0.614	
	0.874	−0.165	−0.457	
	2.0536 ± 0.0002	**2.0102 ± 0.0002**	**2.0031 ± 0.0002**	
O^-–V_{Zn}–Al^{3+}	0.444	0.608	0.658	This work
	−0.182	0.781	−0.598	
	0.877	−0.146	−0.457	

4. Summary

A new W^{5+}-type electron centre created in $ZnWO_4$ by UV- or x-irradiation at 77 K has been found and characterised by EPR and ENDOR. The stability of this centre is explained by a charge-compensating impurity identified as an isolated Al^{3+} ion replacing Zn^{2+}. Comparing the spin densities at the central W nucleus for two similar centres, W^{5+}–Al^{3+}_{Zn} and W^{5+}–Sn^{4+}_{Zn}, one can conclude that in the latter defect the less localised spin density is due to a nearby Zn vacancy providing the charge compensation for Sn^{4+}_{Zn} in the unirradiated sample. Therefore the improved model for the centre is W^{5+}–Sn^{4+}_{Zn}–V_{Zn}.

After x-irradiation at 77 K a new hole-type defect is observed in $ZnWO_4$:Al and identified as an O^-–V_{Zn}–Al^{3+} centre. The lack of any ^{67}Zn SHF interaction indicates that a V_{Zn} is also involved in this centre. The two stronger W SHF interactions suggest that the hole is localised at an oxygen site of B-type, where two W and one Zn neighbours are present (instead of the A-type with two Zn and one W neighbours). The similar $\tilde{\mathbf{g}}$ tensors of all known hole-type defects point to a similar structure, namely O^- in the B position.

The O^-–V_{Zn}–OH^- centre was observed in very high concentration in the $ZnWO_4$:Al system since the precursor V_{Zn}–OH^- complex which charge compensates the Al^{3+} impurity non-locally is available in a relatively high concentration. This allowed the additional determination of the SHF interaction tensors for two regular W neighbours.

The existence of an Al–V_{Zn} related hole-type defect also means that some fraction of the impurity ions is compensated locally by Zn vacancies as well as single Al^{3+} ions charge compensated non-locally. Since these Al^{3+}–V_{Zn} pairs represent overcompensation and are locally negative they are able to capture holes, while isolated Al^{3+} ions due to their extra positive charge capture electrons.

A third hole-type centre with low intensity and quartet SHF is attributed to an O^-–Na_{Zn} defect.

Acknowledgments

This work was supported by the DAAD (Germany), the National Science Research Fund OTKA, Hungary (Grant No T-22859) and the Centre of Excellence Program (Contract No ICA1-2000-70029 EU).

References

[1] Oi T, Takagi K and Fukazawa T 1980 *Appl. Phys. Lett.* **36** 278
[2] Grabmaier B C 1984 *IEEE Trans. Nucl. Sci.* **31** 372
[3] Grassmann H, Moser H-G and Lorenz E 1985 *J. Lumin.* **33** 109
[4] Katscher K (ed) 1980 *Gmelin Handbuch der Anorganishen Chemie, W Ergänzungsband B Oxide* (Berlin: Springer)
[5] Watterich A, Kappers L A and Gilliam O R 1999 *J. Phys.: Condens. Matter* **11** 1333–40
[6] Watterich A, Wöhlecke M, Müller H, Raksányi K, Breitkopf A and Zelei B 1992 *J. Phys. Chem. Solids* **53** 889–95
[7] Watterich A, Gilliam O R, Kappers L A and Raksányi K 1996 *Solid State Commun.* **97** 477–80
[8] Watterich A, Edwards G J, Gilliam O R, Kappers L A, Corradi G, Péter Á and Vajna B 1994 *J. Phys. Chem. Solids* **55** 881
[9] Watterich A, Kovács L, Würz R, Schön F, Hofstaetter A and Scharmann A 2001 *J. Phys.: Condens. Matter* **13** 1595–607
[10] Watterich A and Hofstaetter A 1998 *Solid State Commun.* **105** 357–62
[11] Hofstaetter A, Raksányi K, Scharmann A, Schön F and Watterich A 1993 *Proc. 12th Int.Conf. on Defects in Insulating Materials (Nordkirchen, Germany, 1992)* vol 2, ed O Kanert and J-M Spaeth (Singapore: World Scientific) p 700
[12] Watterich A, Kappers L A and Gilliam O R 1997 *Solid State Commun.* **104** 683–8
[13] Schmidt F and Voszka R 1981 *Cryst. Res. Technol.* **16** K127
[14] Földvári I, Péter Á, Keszthelyi-Lándori S, Capelletti R, Cravero I and Schmidt F 1986 *J. Cryst. Growth* **79** 714
[15] Schofield P F, Knight K S and Cressey G 1996 *J. Mater. Sci.* **31** 2873–7
[16] Wyckoff R W G 1965 *Crystal Structures* 2nd edn, vol 3 (New York: Interscience) pp 41–3
[17] Malicskó L 2001 private communication
[18] Spaeth J-M, Niklas J R and Bartram R H 1992 *Structural Analysis of Point Defects in Solids* (Berlin: Springer) chapter 5.4